

Localized magnon mode of in-plane magnetic vortices in easy-plane magnets

G. M. Wysin*, M. E. Gouvêa and A. S. T. Pires

Departamento de Física, ICEx, Universidade Federal de Minas Gerais, Belo Horizonte, CEP 30161, MG, Brazil

(July 10, 1997, revised Dec. 17, 1997)

We consider localized magnon modes of magnetic vortices in two-dimensional (2D) classical magnets, with exchange or single-ion easy-plane anisotropy stronger than the critical value required to stabilize in-plane vortices. A discrete lattice Ansatz for the structure of a magnon mode on one vortex is analyzed. Its lowest eigenmodes are found to be identical with modes obtained from numerical diagonalization for ferro- (FM) and anti-ferromagnets (AFM), showing that the Ansatz is exact. For the AFM model, one mode is found to be localized, with frequency reaching a size-independent asymptotic limit. A continuum treatment leads to an effective Schrodinger problem that requires a small-radius cutoff due to the singularity of the vortex core. We find, however, that it is not possible to choose this cutoff consistently to recover the exact local mode frequency from the Ansatz. This suggests that strong discrete lattice effects not well-described by the usual continuum approximation always appear from the core of in-plane vortices,

PACS numbers: 75.10.Hk; 75.40.Cx

I. INTRODUCTION

Two-dimensional Heisenberg models with easy-plane (XY) anisotropy continue to attract interest because of the presence of magnetic vortex excitations and their particle-like properties. At finite temperature, however, an individual vortex will be strongly modified by its interaction with magnons, and vice-versa. In particular here we are interested in analyzing magnon modes that are *localized* on a vortex. In the absence of anisotropy, Ivanov¹ found that the Belavin-Polyakov solitons of the 2D isotropic FM model possess a local mode. Spin-wave modes on a vortex in the FM model with easy-plane exchange anisotropy have also been analyzed,² and a similar mode appears, but only the out-of-easy-plane (S^z) spin fluctuations are localized.³ Thus these special FM modes are considered “quasi-local”, and have an anisotropy-dependent frequency that diminishes with increasing system size.³ On the other hand, Ivanov *et al.*⁴ found that for the AFM model with weak easy-plane exchange anisotropy, there is a mode truly localized on a vortex, with frequency determined only by the anisotropy strength. In both FM and AFM cases, these quasi-local and local modes, respectively, are also seen to be associated with^{3,5} the crossover from stable “out-of-plane” vortices (“weak” anisotropy, S^z equals a nonzero function of distance from the vortex core) to stable “in-plane” vortices (“strong” anisotropy, all $S^z = 0$) when the anisotropy strength increases through a critical value.^{6,7} By an Ansatz for the motions of the spins near the core of an in-plane vortex excited by this mode (vortex instability mode, or VIM), Wysin⁸ estimated the critical exchange anisotropy by locating where this mode has zero frequency. Now the Ansatz has been improved,⁹ taking

into account motions of spins far from the vortex core, leading to precise determinations of critical anisotropy, and including also single-ion easy-plane anisotropy. This Ansatz now offers a new opportunity for studying the VIM, especially for the AFM model, which is the focus of this paper.

Except for Ref.,⁹ all of the above calculations considered easy-plane *exchange* anisotropy. Currently there have been fewer vortex mode calculations using a *single-ion* type of easy-plane anisotropy (see Eq. (1) below for the distinction). We cite one in particular. Pereira *et al.*¹⁰ used the vortex-magnon continuous spectrum to calculate the quantum corrections to classical AFM in-plane vortex energy for single-ion anisotropy. Using a continuum description, they also found evidence for a bound state or local mode of an in-plane vortex. There was no mention there whether this mode could be the VIM. We show below, however, that the effective Schrodinger equation for that mode requires a small-radius cutoff in order to have a physically reasonable solution. A primary goal of this work is to analyze further this local mode, for both types of easy-plane anisotropy. We do this by a further analysis of the effective Schrodinger equation, with a cutoff introduced. We also are able to show that this mode is the VIM of the in-plane vortex, regardless of the type of easy-plane anisotropy.

As there is always some freedom and therefore uncertainty about how to put in such a cutoff, however, an analysis of the corresponding discrete lattice problem is important as a control. In this case, the Ansatz for the VIM made by Wysin⁹ to calculate the critical anisotropy can be used to determine both the eigenvalue and eigenfunctions of the in-plane vortex local mode. The Ansatz is based on successively taking into account spins at larger and larger radii from the vortex core, all exactly,

and assuming that the wavefunction for the mode has a simple symmetry that is determined by the underlying lattice symmetry. In fact, while the VIM wavefunction is actually circularly symmetric, Wysin's Ansatz includes both circularly symmetric solutions and solutions with symmetry of the lattice.

The paper is organized as follows: First we present the spin model and Ansatz for a mode on an in-plane vortex on a discrete lattice. The Ansatz is applicable either to the FM model on square, hexagonal and triangular lattices, or to the AFM model on square and hexagonal lattices.¹¹ Results from the Ansatz are presented and compared with other results from exact diagonalization. Then we review the derivation of the continuum limit effective Schrodinger equation for modes on an AFM in-plane vortex. We present the arguments for introduction of a cutoff, and then show the resulting solutions obtained from a shooting method. Finally we compare with the Ansatz results.

II. THE MODEL AND IN-PLANE VORTICES

We consider 2D spin models on a lattice, with easy-plane (XY) anisotropy of exchange type (dimensionless parameter $\delta \geq 0$) and of single-ion type (dimensionless parameter $d \geq 0$), with Hamiltonian:

$$H = J \sum_{\mathbf{n}} \left\{ \mp \frac{1}{2} \sum_{\mathbf{a}} \left[\vec{S}_{\mathbf{n}} \cdot \vec{S}_{\mathbf{n}+\mathbf{a}} - \delta S_{\mathbf{n}}^z S_{\mathbf{n}+\mathbf{a}}^z \right] + d(S_{\mathbf{n}}^z)^2 \right\}, \quad (1)$$

where $J > 0$, subscript \mathbf{n} labels the lattice sites and subscript \mathbf{a} labels the set of displacements to the nearest neighbors. Upper and lower signs here and below correspond to ferromagnetic (FM) and antiferromagnetic (AFM) models, respectively. For description of vortices it is convenient to write the spins as

$$\vec{S}_{\mathbf{n}} = S(\sqrt{1 - m_{\mathbf{n}}^2} \cos \phi_{\mathbf{n}}, \sqrt{1 - m_{\mathbf{n}}^2} \sin \phi_{\mathbf{n}}, m_{\mathbf{n}}). \quad (2)$$

where ϕ is the in-plane angle and $m = S^z/S$ is the out-of-plane component. An in-plane FM vortex at the origin, with vorticity $q = \pm 1$, has $S_{\mathbf{n}}^z = 0$ and $\phi_{\mathbf{n}}^o = \Phi_{\mathbf{n}}^v$, where the static vortex angles $\Phi_{\mathbf{n}}^v$ satisfy the discrete-lattice Laplace-like equation,

$$\sum_{\mathbf{a}} \sin(\Phi_{\mathbf{n}}^v - \Phi_{\mathbf{n}+\mathbf{a}}^v) = 0. \quad (3)$$

This equation is equivalent to the static equation of motion, $\vec{S}_{\mathbf{n}}^z = 0$. In the continuum limit, with small gradients, $(\Phi_{\mathbf{n}}^v - \Phi_{\mathbf{n}+\mathbf{a}}^v) \ll 1$, this equation passes over into the 2D Laplace equation. We solved this equation by first setting the in-plane angles to their continuum vortex values,

$$\Phi_{\mathbf{n}}^v = q \tan^{-1} y/x, \quad (4)$$

and then iteratively setting each spin's xy-components to point along the direction of the effective field due to its neighbors. A similar method was used for all three spin components in Refs.^{4,5} This iteration results in small differences of the discrete solution from the continuum result (4), especially near the vortex core. Typically, the discrete lattice vortex has an energy a few percent (at most) smaller than that obtained when using the continuum expression for the angles.

An in-plane AFM vortex again has $S_{\mathbf{n}}^z = 0$, but compared to the FM vortex, has $\phi_{\mathbf{n}}^o$ modulated according to the sublattice l of site \mathbf{n} . Letting $\Phi_l = 2\pi l/L$, where L is the number of sublattices ($L = 2$ for square and hexagonal lattices, $L = 3$ for triangular lattice), and $l = 0, 1, \dots, (L - 1)$, the AFM vortex has in-plane component $\phi_{\mathbf{n}}^o = \Phi_{\mathbf{n}}^v + \Phi_{l_{\mathbf{n}}}$. The $l_{\mathbf{n}}$ are assigned such that that no neighboring sites have identical values. Note, however, that for the triangular lattice, while we can form the structure of the AFM in-plane vortex, we are not aware of a similar smooth solution for the out-of-plane vortex. It is clear that the frustration in this case makes both the the out-of-plane vortex structure and form of a possible VIM wavefunction difficult if not impossible to consider. Thus the AFM model is considered only on square and hexagonal lattices.

The consideration of in-plane vortex stability shows that the in-plane vortex is stable only under sufficiently strong anisotropy, $\delta > \delta_c$ or $d > d_c$, depending on the form being considered.^{8,9} For a vortex at the center of a finite circular system, the critical values δ_c and d_c depend weakly on the system size, and reach asymptotic limits as shown in Table I. Generally in what follows we consider anisotropy strengths greater than the appropriate critical value, such that the in-plane vortex satisfying (3) is a stable static solution to Hamiltonian (1).

III. THE NORMAL MODE ANSATZ

Here we give details of the normal mode Ansatz introduced in Ref.,⁹ that includes the VIM. We consider simple ways in which the spins in the vortex structure perform small-amplitude oscillations φ and m ,

$$\phi_{\mathbf{n}} = \phi_{\mathbf{n}}^o + \varphi_{\mathbf{n}}, \quad S_{\mathbf{n}}^z = S m_{\mathbf{n}}. \quad (5)$$

The Hamiltonian in terms of these perturbations is

$$H = JS^2 \sum_{\mathbf{n}} \left\{ \mp \frac{1}{2} \sum_{\mathbf{a}} \left[\sqrt{1 - m_{\mathbf{n}}^2} \sqrt{1 - m_{\mathbf{n}+\mathbf{a}}^2} \times \right. \right. \\ \left. \left. \cos(\phi_{\mathbf{n}}^o - \phi_{\mathbf{n}+\mathbf{a}}^o) \cos(\varphi_{\mathbf{n}} - \varphi_{\mathbf{n}+\mathbf{a}}) + \lambda m_{\mathbf{n}} m_{\mathbf{n}+\mathbf{a}} \right] \right. \\ \left. + d m_{\mathbf{n}}^2 \right\}, \quad (6)$$

where $\lambda \equiv 1 - \delta$ is the relative net exchange coupling of the S^z components.

One expects that for any normal mode the perturbations φ and m could have a dependence on the azimuthal

coordinate χ as $e^{il\chi}$, where l is an integer (angular momentum quantum number). For example, the VIM as seen from numerical diagonalization^{4,5} is circularly symmetric, with $l = 0$, or equivalently, has a wavefunction with only a dependence on the radial coordinate r . Thus an Ansatz that includes the VIM need only allow for this possibility, but in fact, can be more general as well. Instead of supposing that φ and m depend only on r , the Ansatz is that they depend on what we call shells or “rings”, where the sites belonging to a given ring are all at the same r , and in addition to this, can be mapped into each other by symmetry operations that depend on the lattice. The FM Ansatz is to assume that all sites on a given ring labeled by a parameter α have the *same* perturbations φ_α and m_α , completely in phase. For the AFM Ansatz on square and hexagonal lattices, it is assumed that sites on the same sublattice on a ring move in phase, with the same φ_α and m_α , while the other sublattice is exactly out of phase with this, having perturbations $-\varphi_\alpha$ and $-m_\alpha$. It is necessary to consider the details of these ring variable definitions on square, hexagonal, and triangular lattices separately.

A. Square Lattice

The vortex is assumed to be at the origin (0,0), centered in a unit cell. Then as shown in Fig. 1, the lattice sites in one quadrant near the vortex core have coordinates $(x, y) = (\frac{a}{2}i, \frac{a}{2}j)$, where a is the lattice constant and i and j are *odd* integers (Fig. 1). Different sets of sites at equal radii from the vortex center can be identified, depending on whether they lie on one of the lines of symmetry $|i| = |j|$ or not. A site with $|i| = |j|$ (on solid line in Fig. 1), can be reflected through the x and y axes to get the four sites $(x, y) = \frac{a}{2}(\pm i, \pm i)$. These four sites then comprise the ring denoted by (i, i) (a solid circle on solid line in Fig. 1). For $|i| \neq |j|$, the eight sites, $(x, y) = \frac{a}{2}(\pm i, \pm j), \frac{a}{2}(\pm j, \pm i)$ related by reflections through the x,y axes and through the (11) directions, comprise a ring denoted (i, j) (a solid circle not on the solid line in Fig. 1). In general, any ring α can be uniquely denoted by the pair $\alpha_{(i,j)} \equiv (i, j)$, with $i > 0$, $j > 0$, and $i \geq j$. Different rings may have identical radii, such as rings (5,5) and (7,1), but we still consider them as independent variables. In this way there is actually some angular dependence that can occur in the normal mode, because the sites in equal radii rings lie in different directions, and the Ansatz is able to produce modes with angular momentum quantum number $l \neq 0$. All rings have either four or eight sites; we denote the number of sites in a ring by $\mu_{(i,j)} = 8 - 4\delta_{i,j}$. To express the perturbed energy of the vortex in terms of the ring variables, it is also useful to define a variable, $c_{\alpha,\alpha'}$, which is the total number of bonds between any pair of rings α and α' . For the square lattice, inspection of Fig. 1 shows that $c_{\alpha,\alpha'} = 8$ between any two neighboring rings and

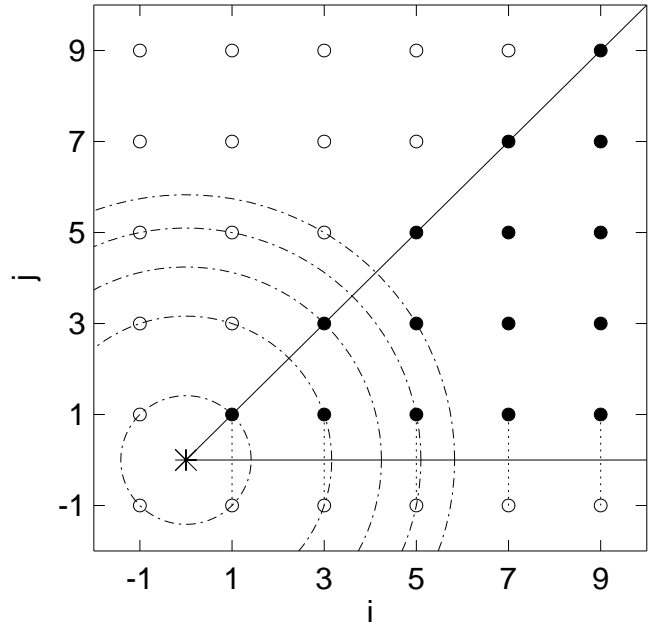


FIG. 1. Ring coordinates (i, j) for square lattice. Only the first few rings are drawn. The vortex center is denoted by *. Solid dots indicate the sites needed to identify the rings, with other sites of a ring (open dots) obtained by appropriate reflections and rotations. Rings with dots on the solid lines have half as many sites as other rings. Dotted lines indicate ring (exchange) self-interaction.

zero otherwise. Also, we note that rings with $j = 1$ always have 4 bonds within that ring (ring self-interaction, dashed lines in the Fig. 1).

B. Hexagonal lattice

The modification to treat lattices other than square is only to make the definitions of the rings appropriately, based on the symmetries of the lattice. For the square lattice, the symmetries allow us to solve the problem using about 1/8 of the full circle. For hexagonal lattice, we get a reduction to 1/12 of the full circle, by defining the rings as follows: Using appropriate orthogonal x and y axes as shown in Fig. 2, the hexagonal lattice sites are located at $(x, y) = (\sqrt{\frac{3}{2}}i, \frac{1}{2}j)a$, where i and j are integers such that $(i + j)$ is even and j is not equal to zero nor equal to any multiple of 3. When $i = j$ (on solid line in Fig. 2), there are six sites at the same radius, all related to each other by 60° rotations, comprising a ring. When $i \neq j$, there are twelve sites at the same radius, related to each other by 60° rotations together with reflections through the line $i = j$, and these sites also comprise a ring. So in general a pair $\alpha = (i, j)$ under

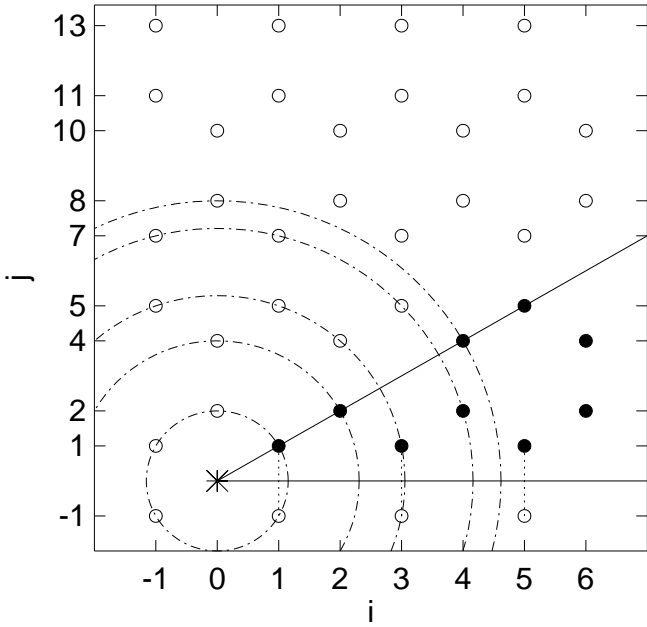


FIG. 2. Ring coordinates (i, j) for hexagonal lattice, notation as in Fig. 1.

the above constraints together with $i > 0, j > 0, i \geq j$ always falls in the first 1/12 of the full circle, and can be used to denote a ring. The number of members of each ring is $\mu_{(i,j)} = 12 - 6\delta_{i,j}$, and the number of bonds between neighboring rings is $c_{\alpha,\alpha'} = \max[\mu_{\alpha}, \mu_{\alpha'}]$. As in the square lattice, only the rings with $j = 1$ have 6 internal bonds or self-interactions.

C. Triangular lattice

Here the symmetry allows a reduction of the problem to 1/6 of the full circle. With orthogonal coordinate axes as in Fig. 3, the triangular lattice sites are located at $(x, y) = (\frac{1}{\sqrt{3}} + \frac{\sqrt{3}}{2}i, \frac{1}{2}j)a$, where i and j are integers such that $(i + j)$ is even. Starting with any site, the other members of its ring are obtained from 120° rotations together with reflection across the x-axis. So a pair $\alpha = (i, j)$ under the above constraints together with $i \geq 0, j \geq 0, y \leq \sqrt{3}x$, always falls in the first 1/6 of the full circle, and can be used to denote a ring. The rings with $j = 0$ and those with $j = 3i + 2$ ($y = \sqrt{3}x$) (on solid lines in Fig. 3) have $\mu_{\alpha} = 3$ (these rings lie on the boundaries of the first 1/6 of the full circle); all other rings have $\mu_{\alpha} = 6$. The number of bonds between neighboring rings is $c_{\alpha,\alpha'} = \max[\mu_{\alpha}, \mu_{\alpha'}]$, except when α or α' is the smallest ring, in which case $c_{\alpha,\alpha'} = 6$. In contrast to the square and hexagonal lattices, here the rings with $j = 1$ and the rings with $j = 3i$ (lying near 60° angle from the x-axis) have 3 internal bonds.

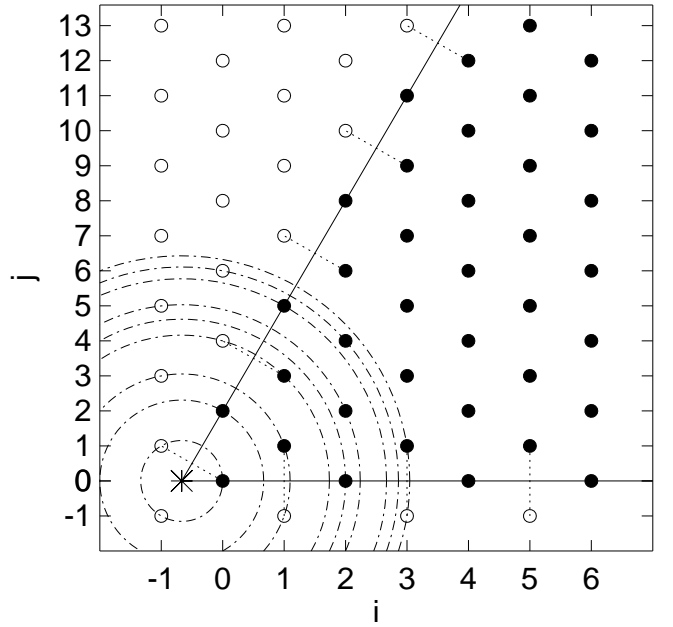


FIG. 3. Ring coordinates (i, j) for triangular lattice, notation as in Fig. 1.

IV. THE ANSATZ DYNAMICS

The Hamiltonian is expressed in terms of the ring variables by the knowledge of the ring couplings $c_{\alpha,\alpha'}$, the ring weights μ_{α} , and the ring self-interactions described above, augmented by the following: We use n_{α} to represent the rings that are neighbors of ring α . We define $s_{\alpha} \equiv 1$ for the rings with self-interaction bonds and $s_{\alpha} \equiv 0$ for all other rings. The rings with self-interaction have n internal bonds, where $n = 4, 6$, and 3 for square, hexagonal and triangular lattices, respectively. For the FM normal mode Ansatz, as described above (Sec. III), we assume that all sites on a ring move exactly in-phase, with the same perturbations, $\varphi_{\alpha}, m_{\alpha}$. For the AFM normal mode Ansatz on square or hexagonal lattices, we assume that all sites of one sublattice of a ring move exactly in-phase, with the same perturbations, $\varphi_{\alpha}, m_{\alpha}$, while the other sublattice has exactly opposite perturbation, $-\varphi_{\alpha}$ and $-m_{\alpha}$. As noted above, this Ansatz actually allows for $l \neq 0$ modes. Now the Hamiltonian can be rewritten as $H = H_{\text{int}} + H_{\text{self}}$, where the interactions between rings, and self-interactions within rings are

$$H_{\text{int}} = -\frac{1}{2}JS^2 \sum_{\alpha, n_{\alpha}} c_{\alpha, n_{\alpha}} \left[\sqrt{1 - m_{\alpha}^2} \sqrt{1 - m_{n_{\alpha}}^2} \times \cos(\Phi_{\alpha}^v - \Phi_{n_{\alpha}}^v) \cos(\varphi_{\alpha} \mp \varphi_{n_{\alpha}}) + \lambda m_{\alpha} m_{n_{\alpha}} \right], \quad (7a)$$

$$H_{\text{self}} = -JS^2 \left\{ \sum_{\alpha} n s_{\alpha} \left[(1 - m_{\alpha}^2) \cos 2\tilde{\Phi}_{\alpha}^v \cos(\varphi_{\alpha} \mp \varphi_{\alpha}) + \lambda m_{\alpha}^2 \right] - d \sum_{\alpha} \mu_{\alpha} m_{\alpha}^2 \right\}. \quad (7b)$$

The Φ_α^v indicate the unperturbed vortex angles Φ^v at the site defining ring $\alpha = (i, j)$. For the self-interactions, it was also necessary to introduce new angles $\tilde{\Phi}_\alpha^v$, which are identical to Φ_α^v , except for the triangular lattice rings with $j = 3i$, where $\tilde{\Phi}_\alpha^v \equiv \Phi_\alpha^v + 2\pi/3$. To obtain H_{self} it is necessary to realize that at pairs of lattice sites in a bond within one ring (for example, consider $(i, 1)$ and $(i, -1)$ on the square lattice), the values of Φ^v differ in sign while φ values are either equal (FM Ansatz, upper signs) or exactly opposite (AFM Ansatz, lower signs). This argument is modified for the $j = 3i$ triangular lattice rings because the bond involved in this interaction that crosses the x axis is only obtained after a $2\pi/3$ rotation of the site (i, j) , see Fig. 3.

The dynamics is derived from the Lagrangian in terms of the ring variables:

$$L = S \sum_{\mathbf{n}} \dot{\phi}_{\mathbf{n}} m_{\mathbf{n}} - H = S \sum_{\alpha} \mu_{\alpha} \dot{\varphi}_{\alpha} m_{\alpha} - H. \quad (8)$$

Euler-Lagrange variation with respect to the ring variables followed by linearization in φ and m leads to equations of motion:

$$S\mu_{\alpha}\dot{m}_{\alpha} = -\frac{\partial H}{\partial \varphi_{\alpha}} \approx -JS^2 \left\{ \sum_{n_{\alpha}} c_{\alpha, n_{\alpha}} \cos(\Phi_{\alpha}^v - \Phi_{n_{\alpha}}^v) \times (\varphi_{\alpha} \mp \varphi_{n_{\alpha}}) + 2ns_{\alpha} \cos 2\tilde{\Phi}_{\alpha}^v (\varphi_{\alpha} \mp \varphi_{\alpha}) \right\}, \quad (9a)$$

$$S\mu_{\alpha}\dot{\varphi}_{\alpha} = \frac{\partial H}{\partial m_{\alpha}} \approx JS^2 \left\{ \sum_{n_{\alpha}} c_{\alpha, n_{\alpha}} \left[\cos(\Phi_{\alpha}^v - \Phi_{n_{\alpha}}^v) m_{\alpha} - \lambda m_{n_{\alpha}} \right] + 2ns_{\alpha} [\cos 2\tilde{\Phi}_{\alpha}^v - \lambda] m_{\alpha} + 2d \mu_{\alpha} m_{\alpha}^2 \right\}. \quad (9b)$$

These equations could be expressed using square matrix operators \mathcal{F} and \mathcal{M} ,

$$\dot{\varphi}_{\alpha} = JS \sum_{\alpha'} \mathcal{F}_{\alpha, \alpha'} m_{\alpha'}, \quad \dot{m}_{\alpha} = JS \sum_{\alpha'} \mathcal{M}_{\alpha, \alpha'} \varphi_{\alpha'}. \quad (10)$$

One sees that there are solutions with $e^{i\omega t}$ time dependence, and that the equations separate;

$$-\omega^2 \begin{bmatrix} \varphi \end{bmatrix} = \mathcal{F}\mathcal{M} \begin{bmatrix} \varphi \end{bmatrix}, \quad -\omega^2 \begin{bmatrix} m \end{bmatrix} = \mathcal{M}\mathcal{F} \begin{bmatrix} m \end{bmatrix}, \quad (11)$$

where $\begin{bmatrix} \varphi \end{bmatrix}$ and $\begin{bmatrix} m \end{bmatrix}$ are column matrices describing the eigenvector of mode, and ω is the frequency in units of JS . The frequencies are obtained from the square root of eigenvalues of the product matrix, $\mathcal{M}\mathcal{F}$.

A. Two Rings for Square Lattice

Although it is not too accurate, we can get an idea of how the VIM behaves by using only two rings, for the

square lattice, as an example. We allow rings $(1, 1)$ and $(3, 1)$ to be dynamic, while the spins of all rings at larger radii are held fixed in the directions of the static in-plane vortex. We also use the unrelaxed in-plane structure, Eq. (4), for simplicity; the error caused by this approximation is much smaller than the error due to using such a small number of rings. Then the matrices \mathcal{M} and \mathcal{F} become

$$\mathcal{M} = \begin{pmatrix} -2A_s & \pm 2A_s \\ \pm A_s & -A_s(2 + 2C_s + A_s \mp A_s) \end{pmatrix} \quad (12a)$$

$$\mathcal{F} = \begin{pmatrix} 2(A_s + d - \lambda) & -2\lambda \\ -\lambda & B_s + 2d - \lambda \end{pmatrix} \quad (12b)$$

where the notation, as in Ref.⁸ is

$$A_s = \frac{2}{\sqrt{5}}, \quad B_s = \frac{4}{\sqrt{5}} \left(1 + \frac{1}{\sqrt{5}} + \frac{2}{\sqrt{13}} \right), \quad C_s = 2\sqrt{13}. \quad (13)$$

A straightforward calculation of the eigenvalues of matrix $\mathcal{M}\mathcal{F}$ can be performed, concentrating on the cases when the anisotropy is just above critical ($\delta_c \approx 0.2843$, $d_c \approx 0.4011$), for either pure exchange anisotropy ($d = 0$, $\delta > \delta_c$) or pure single-ion anisotropy ($\delta = 0$, $d > d_c$). For both types of anisotropy, and for both the FM and AFM models, there is one mode found, whose frequency goes to zero at the respective critical anisotropy. Clearly, this is the VIM. For anisotropy close to the critical value, we find that ω has a square root dependence on the deviation of the anisotropy away from the critical value;

$$\omega/JS = B_d \sqrt{d - d_c}, \quad \omega/JS = B_{\delta} \sqrt{\delta - \delta_c}. \quad (14)$$

The coefficients B_d and B_{δ} in this low approximation are shown in Table II. The mode's frequency tends to grow more quickly with anisotropy for the AFM model compared to the FM model, and also grows more quickly (in some sense) for exchange anisotropy compared to single-ion anisotropy. These calculations are next improved by determining the VIM for an arbitrary number of rings numerically.

V. NUMERICAL SOLUTION FOR ANSATZ EIGENMODES

Primarily we are interested in finding the lowest eigenmode(s) of Eqs. (10), for some finite number of rings, N , which is easily and quickly done by a relaxation method. A little consideration shows that the matrices $\mathcal{A} = \mathcal{M}\mathcal{F}$ and $\mathcal{A}^T = \mathcal{F}\mathcal{M}$ are not necessarily Hermitian. This means that it is necessary to consider both the right and left eigenvectors of \mathcal{A} . Consider the eigenvectors for the out-of-plane motion of a mode labeled by k . We suppose there is a right (column) eigenvector, $\begin{bmatrix} m_k \end{bmatrix}$, and a

left (row) eigenvector with the same eigenvalue, $[{}_k m]$, which satisfy,

$$\mathcal{A} \begin{bmatrix} m_k \end{bmatrix} = -\omega_k^2 \begin{bmatrix} m_k \end{bmatrix}, \quad [{}_k m] \mathcal{A} = -\omega_k^2 [{}_k m]. \quad (15)$$

For the left eigenvectors, we place the subscript k to the left side to stress that $[{}_k m]$ is not just the transpose of $\begin{bmatrix} m_k \end{bmatrix}$. If both these eigenvectors are known, the eigenfrequency is obtained easily,

$$\omega_k^2 = -\frac{[{}_k m] \mathcal{A} \begin{bmatrix} m_k \end{bmatrix}}{[{}_k m] \begin{bmatrix} m_k \end{bmatrix}}. \quad (16)$$

Generally we expect real frequencies, and so the eigenvalues of \mathcal{A} are usually negative (except if anisotropy strength is less than critical, in which case the VIM has an imaginary frequency.)

A way in which the eigenvectors can be obtained is by considering \mathcal{A} as effecting a time evolution in fictitious time τ according to

$$\frac{d}{d\tau} \begin{bmatrix} m \end{bmatrix} = \mathcal{A} \begin{bmatrix} m \end{bmatrix}. \quad (17)$$

From a randomly chosen initial configuration of the matrix $\begin{bmatrix} m \end{bmatrix}$, with overlap $c_k = [{}_k m] \begin{bmatrix} m(0) \end{bmatrix}$ on all eigenmodes, the general solution is simple,

$$\begin{bmatrix} m \end{bmatrix} = \sum_k c_k \begin{bmatrix} m_k \end{bmatrix} e^{-\omega_k^2 \tau}, \quad (18)$$

as verified by using Eq. (15) and Eq. (17). It is clear that for large τ , the right eigenvector with the smallest ω^2 will dominate. A similar process can be applied to get the left eigenvector of the lowest mode, and thus ω_k is known from Eq. (16). We used a standard fourth order Runge-Kutta time integration scheme with fixed time step $\Delta\tau = 0.04$ to produce this time evolution. The choice of time step is not crucial, but only needs to be small enough to ensure stability.

To get higher modes, it is only necessary to enforce that the current eigenvectors $[{}_k m]$ and $\begin{bmatrix} m_k \end{bmatrix}$ being found are orthogonal to all previously found lower states q , applying the constraints

$$[{}_q m] \begin{bmatrix} m_k \end{bmatrix} = 0, \quad [{}_k m] \begin{bmatrix} m_q \end{bmatrix} = 0. \quad (19)$$

The Gram-Schmidt orthogonalization scheme was used to apply this constraint.

Once the eigenvectors for out-of-plane motion are known, the in-plane fluctuations are determined. By using Eq. (10) with $e^{i\omega_k t}$ time dependence, we have

$$\begin{bmatrix} \varphi_k \end{bmatrix} = \frac{1}{i\omega_k} \mathcal{F} \begin{bmatrix} m_k \end{bmatrix}. \quad (20)$$

This shows that the in-plane fluctuations are exactly 90° out-of-phase with the out-of-plane fluctuations. This will give the correct normalization of $\begin{bmatrix} \varphi \end{bmatrix}$ relative to $\begin{bmatrix} m \end{bmatrix}$. In Ref.,³ the correct absolute normalization has been shown to be

$$i \sum_{\mathbf{n}} (m_{\mathbf{n}}^* \varphi_{\mathbf{n}} - m_{\mathbf{n}} \varphi_{\mathbf{n}}^*) = 1, \quad (21)$$

where the sum is over the original lattice site variables. Converting this to ring variables leads to the absolute normalization condition

$$\sum_{\alpha} 2\mu_{\alpha} (\begin{bmatrix} m_k \end{bmatrix})_{\alpha} (\mathcal{F} \begin{bmatrix} m_k \end{bmatrix})_{\alpha} = \omega_k, \quad (22)$$

where the notation $(\begin{bmatrix} m_k \end{bmatrix})_{\alpha}$ indicates the α^{th} component of column matrix $\begin{bmatrix} m_k \end{bmatrix}$.

For this nearest neighbor interaction problem, the matrices \mathcal{M} and \mathcal{F} are very sparse, there being at most $z+1$ nonzero elements in each row, where z is the coordination number of the lattice ($z = 4, 3, 6$ for square, hexagonal, triangular lattices, respectively). The number of nonzero elements in a row is even less than $z+1$ for those rows corresponding to rings with self-interactions. Thus, it is advantageous in terms of memory and cpu time if only these nonzero elements are saved, together with their column locations, which is equivalent to the information in the near neighbor table. (The matrix is now stored as a $N \times (z+1)$ array.) Then the speed of matrix multiplication by \mathcal{M} or by \mathcal{F} is significantly enhanced. The fictitious time evolution in Eq. (17), which requires repeated matrix multiplications with \mathcal{A} , can be carried out now by successively multiplying by matrices \mathcal{M} and \mathcal{F} , stored in their compact forms. In this way it is possible to solve fairly quickly for the modes on rather large lattices (system radius R greater than 50 lattice constants), and in general the algorithm will be limited by the speed of the cpu (or patience of the computer operator) rather than by the available memory.

A. FM Ansatz Spectra

Some typical results from this relaxation scheme for the three different lattices are presented in Fig. 4. There we compare the frequencies of the lowest four modes of a vortex in square, hexagonal and triangular FM systems, using single-ion anisotropy, and plotting the modes vs. a reduced anisotropy, $\sqrt{d-d_c}$. We compare systems with similar radii: square lattice with $N = 415$ (3228 sites), $R = 31.98$ (largest ring is (63, 11)), hexagonal lattice with $N = 216$ (2460 sites), $R = 32.00$ (largest ring is (32, 32)), and triangular lattice with $N = 637$ (3711 sites), $R = 31.97$ (largest ring is (34, 22)). For this type of Dirichlet boundary condition, the lowest mode is the VIM.

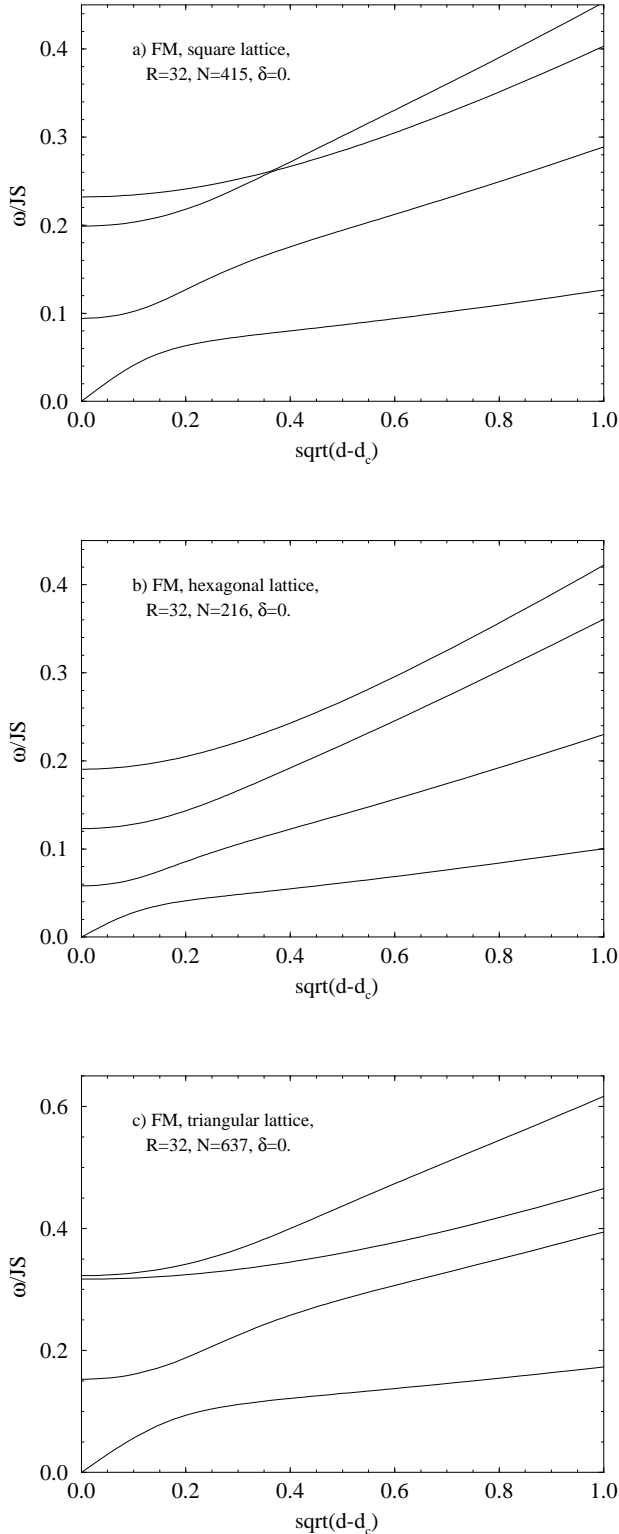


FIG. 4. Typical discrete Ansatz calculation of four lowest modes of FM vortex systems with radius $R = 32$, for single-ion anisotropy, on a) square, ($N = 415$), b) hexagonal ($N = 216$) and c) triangular ($N = 637$) lattice systems.

For very small reduced anisotropy, the VIM frequency has an approximately linear behavior as in Eq. (14), but with the coefficient B_d dependent on the lattice, essentially a result of the different packings. This coefficient and the VIM frequency *decrease* for larger R , approximately as $1/R$, indicating that the mode is not localized. For anisotropy farther away from the critical value, there is another linear behavior of the VIM frequency on reduced anisotropy, with a different slope. Similar results hold for the case of exchange anisotropy. For the system radius $R \approx 32$, we show in Table III the fitting coefficients B_d and B_δ of Eq. (14) in the limit of small single-ion as well as exchange anisotropy.

For square lattice systems with $R \leq 20$, we compared these results with exact diagonalization for the mode spectrum. The mode frequencies and wavefunctions from the Ansatz calculation are identical with some of the modes from numerical diagonalization. However, the diagonalization produces the full spectrum, and includes certain modes with dependence on azimuthal coordinate χ that are impossible to describe by the Ansatz (i.e., modes with angular dependence within the rings themselves, such as the vortex translational modes). For square lattice systems with $R > 20$, the diagonalization scheme is unusable, due to its extreme memory and cpu requirements, and relaxation schemes must be used.

B. AFM Ansatz Spectra

The AFM model is more interesting than the FM model to us here, because of the possibility of localized modes on the vortex, as has been found for the out-of-plane AFM vortices.⁴ Also, the AFM continuum limit equations describing in-plane and out-of-plane spin fluctuations de-couple easily, leading to a clearer analytic treatment with which to compare the Ansatz results.

We show the AFM Ansatz results, for single-ion anisotropy, for the same lattice sizes as used in the FM calculations, in Fig. 5, and for exchange anisotropy, in Fig. 6. For anisotropy very close to critical, the VIM is the lowest mode, while for larger anisotropy, other modes from the acoustic spinwave spectrum can lie lower than the VIM. For the AFM, the VIM mode frequency can be fit extremely well for small reduced anisotropy according to Eq. (14). This result is the same as for the FM model, however, with the important distinction that for the AFM the parameters B_d and B_δ are essentially independent of the system size, except for an extremely small number of rings. Also, the AFM VIM dispersion relation is distinctly more linear than that for the FM model, disregarding the mode crossings. The results are summarized in Table III. The size independence of B_d and B_δ shows that the VIM here is a truly localized mode, which we have also confirmed from inspection of the wavefunctions, as well as comparison with the continuum theory of the next section.

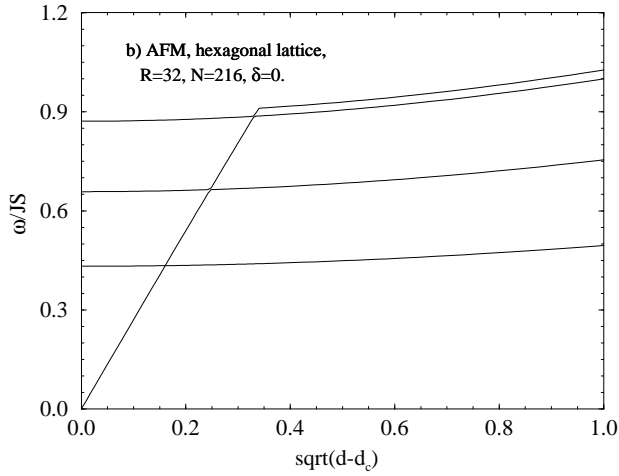
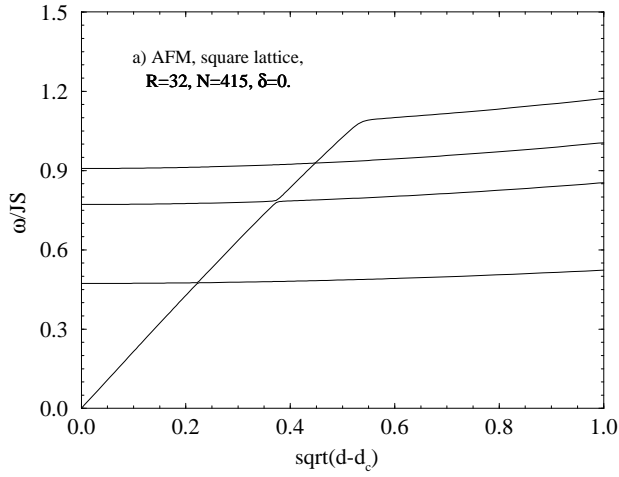


FIG. 5. Typical discrete Ansatz calculation of four lowest modes of AFM vortex systems with radius $R = 32$, for single-ion anisotropy, on a) square, ($N = 415$) and b) hexagonal ($N = 216$) lattice systems.

VI. CONTINUUM AFM NORMAL MODES

A. Square Lattice

For two-sublattice models, the AFM continuum theory can be formulated¹² by writing the spins as

$$\vec{S}_{\mathbf{n}} = \pm S \left(\sin(\Theta_{\mathbf{n}} \pm \theta_{\mathbf{n}}) \cos(\Psi_{\mathbf{n}} \pm \psi_{\mathbf{n}}), \right. \\ \left. \sin(\Theta_{\mathbf{n}} \pm \theta_{\mathbf{n}}) \sin(\Psi_{\mathbf{n}} \pm \psi_{\mathbf{n}}), \cos(\Theta_{\mathbf{n}} \pm \theta_{\mathbf{n}}) \right), \quad (23)$$

where here \pm refers to the two sublattices, “large” angles Ψ and Θ describe AFM order, and “small” angles ψ and θ describe the deviations therefrom (FM order). Then under the assumptions of low frequencies, small gradients

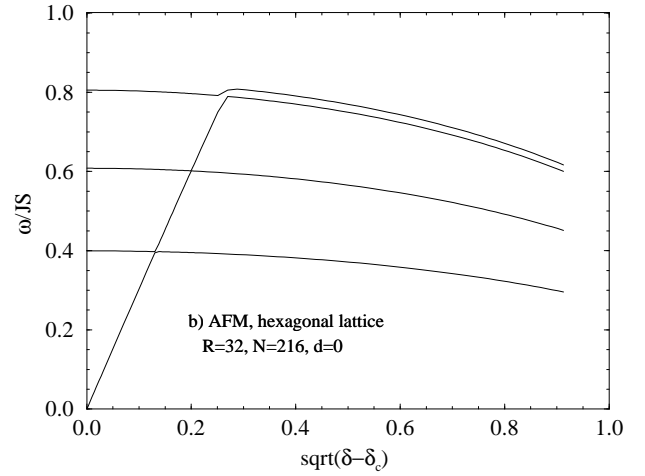
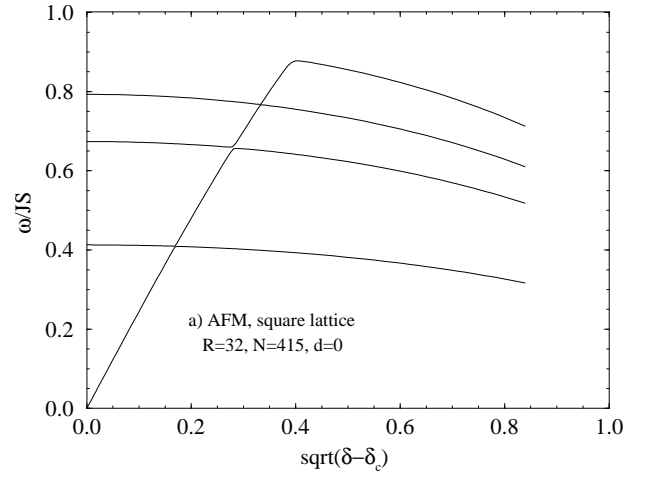


FIG. 6. Typical discrete Ansatz calculation of four lowest modes of AFM vortex systems with radius $R = 32$, for exchange anisotropy, on a) square, ($N = 415$) and b) hexagonal ($N = 216$) lattice systems.

$\nabla\Psi$ and $\nabla\Theta$, and $\psi \ll 1$ and $\theta \ll 1$, the equations of motion for the square lattice from Hamiltonian (1) are¹³

$$\nabla^2\Psi - \frac{1}{c^2} \frac{\partial^2\Psi}{\partial t^2} + 2 \cot\Theta \left[\nabla\Theta \cdot \nabla\Psi - \frac{1}{c^2} \frac{\partial\Theta}{\partial t} \frac{\partial\Psi}{\partial t} \right] = 0, \quad (24a)$$

$$\nabla^2\Theta - \frac{1}{c^2} \frac{\partial^2\Theta}{\partial t^2} - \sin\Theta \cos\Theta \left[|\nabla\Psi|^2 - \frac{1}{c^2} \left(\frac{\partial\Psi}{\partial t} \right)^2 + \Delta \right] = 0, \quad (24b)$$

$$\psi = \frac{1}{8JS} \csc\Theta \frac{\partial\Theta}{\partial t}, \quad (24c)$$

$$\theta = -\frac{1}{8JS} \sin \Theta \frac{\partial \Psi}{\partial t}, \quad (24d)$$

where $c^2 = 8(JS)^2$ is the long-wavelength spinwave velocity, and Δ is a generic anisotropy, or gap of the optical spinwave branch,

$$\Delta = 4\delta + 2d. \quad (25)$$

Now an in-plane AFM vortex has $\Theta = \Theta_v = \pi/2$, $\Psi = \Phi_v = q \tan^{-1} y/x$, with $\theta = \psi = 0$. As in Eq. (5), we assume small-amplitude oscillations at frequency ω about this structure, $\Theta = \Theta_v + \xi$, $\Psi = \Phi_v + \eta$, and $\theta \neq 0$, $\psi \neq 0$ given from Eqs. (24c) and (24d). The linearized dynamic equations for ξ and η are separated Schrodinger-like equations:

$$-\nabla^2 \xi + V(r) \xi = \left(\frac{\omega}{c}\right)^2 \xi, \quad (26a)$$

$$-\nabla^2 \eta = \left(\frac{\omega}{c}\right)^2 \eta. \quad (26b)$$

The effective potential for the ξ wavefunction is

$$V(r) = \Delta - |\nabla \Phi_v|^2 = \Delta - \frac{1}{r^2}. \quad (27)$$

Here it is interesting to note that exchange (δ) and single-ion (d) anisotropy enter in the same place, the only distinction being the different factors of 4 and 2 in the definition [Eq. (25)] of Δ . The two decoupled equations relate to the optical and acoustic spinwave branches. A short calculation using Eqs. (23), (24c) and (24d) shows that in the notation of Eq. (2) the individual sublattices A and B have the following fluctuations:

$$\phi_A = \Phi_v + \eta + \frac{1}{8JS} \frac{\partial \xi}{\partial t}, \quad m_A = -\xi + \frac{1}{8JS} \frac{\partial \eta}{\partial t}, \quad (28a)$$

$$\phi_B = \Phi_v + \eta - \frac{1}{8JS} \frac{\partial \xi}{\partial t}, \quad m_B = \xi + \frac{1}{8JS} \frac{\partial \eta}{\partial t}, \quad (28b)$$

Therefore, the field ξ describes a purely optical or AFM type of motion, while the field η describes a purely acoustic or FM type of motion. As seen in (26b), the η field is not affected by the vortex, has spinwave dispersion $\omega = ck$, and can produce no bound state.

Next we consider whether there can be a bound state of the ξ field. The potential (27) diverges negatively at the origin, suggesting the possibility of a bound state. In the region far from the vortex, we see that the optical spinwave branch has a gap in the dispersion relation, $(\omega/c)^2 = \Delta + k^2$; we look for modes with $(\omega/c)^2$ lying in the gap. Based on the Ansatz and diagonalization calculations for the VIM, we look for circularly symmetric solutions, $\xi(r, \chi) \rightarrow \xi(r)$. Then Eq. (26a) can be put into the form,

$$\left[\frac{d^2}{dx^2} + \frac{1}{x} \frac{d}{dx} + \frac{1}{x^2} - 1 \right] \xi(x) = 0, \quad (29)$$

where $x = \sqrt{\Delta - (\omega/c)^2} r$. Now unfortunately, the equation has no natural length scale, and there is no condition to determine the appropriate eigenvalue, ω , and so there is no bound state solution. If one chooses a frequency at the top of the gap, $(\omega/c)^2 = \Delta$, a mathematical solution of (26a), $\xi(r) \propto \cos \ln(r)$, was mentioned in Ref.,¹⁰ but this solution oscillates wildly as one approaches the origin, and is not a bound state.

The problem is that the effective potential of the discrete lattice problem cannot really diverge negatively, but instead, must reach a finite limit at the vortex core. Here we used the function $1/r^2$ to describe the continuum version of $|\nabla \Phi_v|^2$, but it is clear that on the square lattice, this quantity cannot get much bigger than $(\pi/\sqrt{2})^2$ (consider two diagonal sites in first ring near core). Therefore, we should try to account for this in the continuum theory, and the simplest ways to do this are either to introduce a cutoff, or, to modify the potential to avoid the divergence. We consider a small change in the potential:

$$V(r) = \begin{cases} \Delta - \frac{1}{r_o^2} & \text{for } r < r_o \\ \Delta - \frac{1}{r^2} & \text{for } r > r_o \end{cases} \quad (30)$$

where r_o is a cutoff parameter. While this is a somewhat arbitrary modification, it is physically motivated by the saturation of $|\nabla \Phi_v|^2 \sim 1/r_o^2$ near the vortex core, and we should expect that $r_o \approx \sqrt{2}/\pi$ is reasonable.

1. Variational Calculation

Using potential (30) in Eq. (26a), we have essentially set the length scale to r_o . Now one can try a variational solution, assuming a localized wavefunction,

$$\xi(r) = e^{-\gamma r}. \quad (31)$$

We try to minimize the ‘‘energy’’ given by

$$E = (\omega/c)^2 = \frac{\int d^2 r [|\nabla \xi|^2 + V(r)\xi^2]}{\int d^2 r \xi^2}, \quad (32)$$

with respect to variational parameter γ . A short calculation leads to the results

$$E = \Delta - [1 - (y_o + 1)e^{-y_o}] \frac{1}{r_o^2} \approx \Delta - \frac{0.236}{r_o^2}, \quad (33)$$

$$\gamma = \frac{y_o}{2r_o} \approx \frac{0.4615}{r_o}, \quad (34)$$

where $y_o \approx 0.9231$, is the solution to the integral equation,

$$\int_{y_o}^{\infty} dx \frac{e^{-x}}{x} = \frac{1}{4}. \quad (35)$$

This calculation shows that a bound state is found within the spinwave gap, although the actual frequency depends

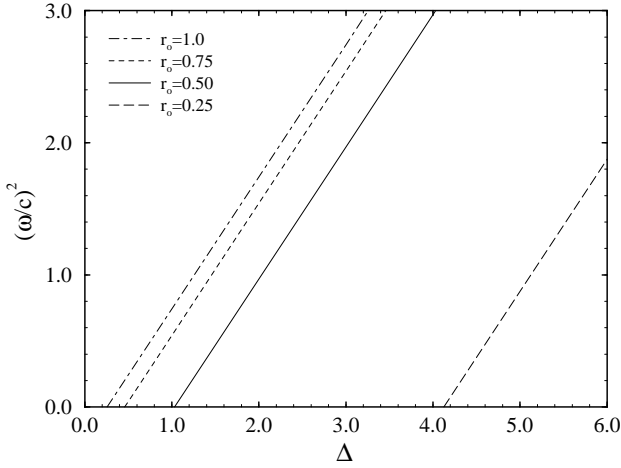


FIG. 7. Squared VIM frequencies $(\omega/c)^2$ vs. anisotropy Δ , from the shooting solutions of Eq. (26a), using $R = 10.0$, $N_{\text{grid}} = 20000$, for indicated cutoffs r_o .

strongly on the cutoff parameter, r_o . Furthermore, it also recovers a critical anisotropy; the energy becomes negative and therefore ω becomes imaginary, signaling an instability of the in-plane vortex, if

$$\Delta < \Delta_c = \frac{0.236}{r_o^2}. \quad (36)$$

This gives the respective critical anisotropies,

$$\delta_c = \frac{1}{4}\Delta_c = \frac{0.236}{4r_o^2}, \quad d_c = \frac{1}{2}\Delta_c = \frac{0.236}{2r_o^2}. \quad (37)$$

We also see that for $\Delta > \Delta_c$, the frequency of this mode varies as

$$\omega/c = \sqrt{\Delta - \Delta_c}, \quad (38)$$

giving corresponding results for the two anisotropy types,

$$\omega = \sqrt{2} c \sqrt{d - d_c}, \quad \omega = 2c \sqrt{\delta - \delta_c}. \quad (39)$$

These are similar in form to the discrete theory, however, the magnitudes are more than a factor of two too large. In this continuum theory, although the values of δ_c and d_c depend on the choice of the cutoff, their ratio is determined: $d_c/\delta_c = 2$, which is larger than the discrete result, $d_c/\delta_c = 1.581$. Therefore we cannot choose r_o such that both critical anisotropies are simultaneously matched to the discrete theory. The choice $r_o = 0.446$ results in $\delta_c = 0.297$, and the choice $r_o = 0.502$ results in $d_c = 0.469$. These cutoffs are comparable to the expected value of $\sqrt{2}/\pi = 0.450$, however, they are somewhat larger than the typical cutoff of $r_o \approx 0.22$ one gets by fitting the energy of the in-plane vortex on a lattice to the continuum form, $E_v = \pi \ln(R/r_o)$, where R is the system radius¹⁴.

The variational solution required a guess for the form of the ξ wavefunction. Here we consider a numerical solution of Eq. (26a) by a shooting method, using the potential with the cutoff, Eq. (30). The method is standard,¹⁵ and requires as an input the number of grid points N_{grid} from $r = 0$ to the maximum radius $r = R$, as well as the generic anisotropy Δ and cutoff r_o . For the integration of the differential equation, we separated it into two first order equations, and used a fourth order Runge-Kutta scheme, with the boundary conditions, $\xi(0) = 1$, $\xi(R) = 0$.

In Fig. 7 we show some typical values of $(\omega/c)^2$ vs. Δ for various r_o , using $R = 10.0$ and $N_{\text{grid}} = 20,000$. There is a linear relationship between $(\omega/c)^2$ and Δ . It is simply a consequence of the linear dependence of $V(r)$ in Eq. (30) on Δ . From these results, we once again recover the critical anisotropy where $(\omega/c)^2$ goes to zero, and can again write the general result as in Eq. (38), where to fairly high precision, the values of critical anisotropy are found to be inversely proportional to the square of the cutoff,

$$\Delta_c = \frac{0.25777}{r_o^2}, \quad (40)$$

and $\delta_c = \Delta_c/4$, $d_c = \Delta_c/2$. This shows that the variational calculation was fairly reliable. The eigenfrequencies here are also given by Eq. (39). This translates into the coefficients, $B_d = \sqrt{2}c/JS = 4$, and $B_\delta = 2c/JS = 4\sqrt{2}$, as defined in (14). Once again, the the continuum result for ω (with factor of $c = \sqrt{8}JS$) is about two times larger than that found from the discrete lattice calculations, see Table III.

To try to see why there is this discrepancy, we show in Fig. 8 a comparison of the ξ wavefunction obtained from the shooting solution, with that obtained from the discrete solution. We adjusted the cutoff r_o to a value that gives the correct d_c for $\delta = 0$, and show the case $d = 0.50$. Surprisingly, the two results agree very well. The primary difference is simply that the discrete solution points cannot cover enough of the continuum curve, especially near the origin, where the continuum solution is largest. It appears that the discrepancy really is a result of the limited ability of the continuum limit to describe the static vortex spin field near the vortex core.

B. Hexagonal Lattice

It is instructive to compare these results with similar continuum limit calculations on the hexagonal lattice. For the two-sublattice hexagonal lattice, a parameterization of the spins as in Eq. (23) will lead to continuum equations similar to those in (24), but with modified generic anisotropy, or gap Δ , and spinwave velocity c .

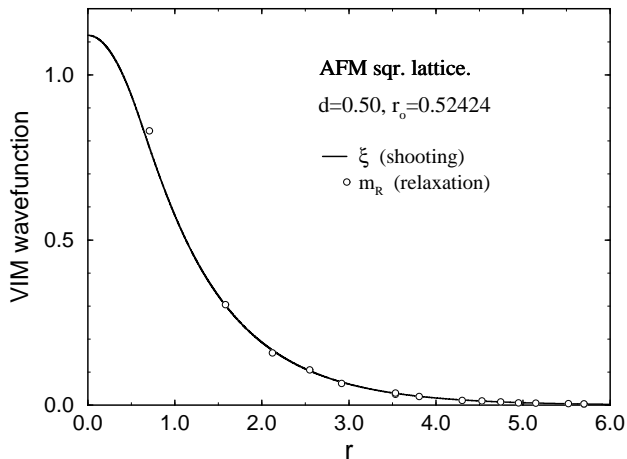


FIG. 8. Comparison of $\xi(r)$ wavefunction for the AFM VIM on square lattice from the shooting solution (solid) with the Ansatz discrete lattice right eigenvector $[m_R]$ (circles). We used $\delta = 0$, $d = 0.50$, where $d_c = 0.4689\dots$. The shooting used $N_{\text{grid}} = 20000$, $R = 10.0$, $r_o = 0.52424$ (to give correct discrete d_c). The Ansatz solution is for $N = 43$ rings.

The effective Schrodinger-like Eqs. (26) and the shooting solutions presented in Fig. 7 also still apply. Thus it suffices for our purpose here to determine the effective Δ and c from the AFM spinwave dispersion relation for the hexagonal lattice, in the absence of a vortex. A short standard calculation shows that for discrete wavevector \mathbf{q} , the spinwaves have the following two-branch dispersion:

$$\left(\frac{\omega}{c}\right)^2 = 2 \left[1 + \frac{2}{3}d - (1 - \delta)|\gamma_{\mathbf{q}}|^2 \pm \left(\delta + \frac{2}{3}d\right)|\gamma_{\mathbf{q}}| \right], \quad (41)$$

where $c = \frac{3}{\sqrt{2}}JS$ is the spinwave velocity at the isotropic limit, and

$$\gamma_{\mathbf{q}} = \frac{1}{3} \sum_{\mathbf{a}} \exp(i\mathbf{q} \cdot \mathbf{a}), \quad (42)$$

with hexagonal near neighbor lattice displacements $\mathbf{a} = (0, -1), (\frac{\sqrt{3}}{2}, \frac{1}{2}), (-\frac{\sqrt{3}}{2}, \frac{1}{2})$. At long wavelengths, $q \ll 1$, the two branches have continuum dispersion relations:

$$\left(\frac{\omega_+}{c}\right)^2 = 4\delta + \frac{8}{3}d + \left(1 - \frac{3}{2}\delta - \frac{1}{3}d\right)q^2, \quad (43a)$$

$$\left(\frac{\omega_-}{c}\right)^2 = \left(1 - \frac{1}{2}\delta + \frac{1}{3}d\right)q^2. \quad (43b)$$

Therefore the appropriate gap is $\Delta = 4\delta + \frac{8}{3}d$, with rather unexpected coefficients on the two anisotropy types. Applying Eq. (38), this then implies the frequency coefficients, $B_d = \sqrt{8/3}c/JS = 2\sqrt{3}$, $B_\delta = 2c/JS = 3\sqrt{2}$.

These are compared with the discrete Ansatz results in Table III. This continuum approach again overestimates these frequency coefficients, although the discrepancy for the hexagonal lattice is less than that appearing for the square lattice.

VII. DISCUSSION AND CONCLUSIONS

We have described an Ansatz for certain spinwave modes in the presence of a magnetic *in-plane* vortex. This Ansatz essentially gives the exact eigenfrequencies of the VIM modes for the three types of lattices discussed. We were able to determine the frequency behavior of this mode for anisotropy strengths greater than those necessary for stabilizing the in-plane vortex. In particular for the AFM model, the VIM mode frequency ω/JS exhibits a linear dependence on the reduced anisotropy $\sqrt{d - d_c}$ or $\sqrt{\delta - \delta_c}$ over a fairly large range of anisotropy. In the FM model the VIM frequency has a linear dependence on reduced anisotropy only over a very limited range, and in fact, appears to be composed of two separate nearly straight segments. The fitting coefficients B_d and B_δ [Eq. (14)] for the FM model decrease with increasing system size, which reflects the fact that the FM VIM mode really is not localized on the vortex, but instead, is spread over the entire system (quasi-local). For the AFM VIM mode, these coefficients are quite independent of the system size, demonstrating that the mode is indeed localized on the vortex. However, the continuum theory gives considerably larger values for these coefficients of the AFM model, for both the square and hexagonal lattices. We do not presently have a good understanding of the reason for this, but suspect that it only reflects the fact that continuum theory is poor at describing the spin fluctuations near the vortex core, where the usual replacement of differences by continuous gradients is very inaccurate.

The introduction of a cutoff parameter r_o into the continuum theory was necessary to produce a mathematically well-behaved solution, however, there is no *a priori* device to choose this cutoff. This is unfortunate since the choice of the cutoff determines the critical anisotropies of the continuum theory, however, the cutoff plays no role in determining the coefficients B_d and B_δ . The latter are determined only by parameters of the spinwave dispersion: the spinwave velocity and the gap as a function of the anisotropies, and for this reason they offered a good way to compare the continuum and discrete results.

VIII. ACKNOWLEDGEMENTS

GMW gratefully acknowledges the hospitality of M. E. Gouvêa and A. S. T. Pires at UFMG. This work was supported by NSF/CNPq International Grant INT-9502781, NSF Grant DMR-9412300, and a FAPEMIG Grant for Visiting Researchers.

TABLE I. Critical anisotropies from Ansatz using $N = 1200$ rings.

Lattice	δ_c	d_c
square	0.29659050564	0.46896252032
hexagonal	0.16704411814	0.22120912667
triangular	0.38714358619	0.83911886856

TABLE II. Approximate VIM frequency coefficients [Eq. (14)] for square lattice using $N = 2$ rings.

Model	B_δ	B_d
FM	1.64	1.38
AFM	2.29	2.01

TABLE III. Weak anisotropy VIM frequency coefficients [Eq. (14)] for radius $R = 32$, as described in the text.

Model	B_δ	B_d
FM (sqr)	0.66	0.45
FM (hex)	0.39	0.32
FM (tri)	1.07	0.60
AFM (sqr)	2.45	2.15
AFM (sqr cont.)	$4\sqrt{2} \approx 5.66$	4
AFM (hex)	3.04	2.71
AFM (hex cont.)	$3\sqrt{2} \approx 4.24$	$2\sqrt{3} \approx 3.46$

* Permanent Address: Department of Physics, Kansas State University, Manhattan, KS 66506-2601. [email: *wysin@phys.ksu.edu*].

- ¹ B.A. Ivanov, JETP Lett. **61**, N11 (1995).
- ² B.V. Costa, M.E. Gouvêa and A.S.T. Pires, Phys. Lett. A **165**, 179 (1992); A. Pereira, A.S.T. Pires and M.E. Gouvêa, Solid State Commun. **86**, 187 (1993); H.-J. Schnitzer, Ph.D. thesis, Univ. Bayreuth (1997).
- ³ G.M. Wysin and A.R. Völkel, Phys. Rev. B **52**, 7412 (1995).
- ⁴ B.A. Ivanov, A.K. Kolezhuk and G.M. Wysin, Phys. Rev. Lett. **76** (1996) 511.
- ⁵ G.M. Wysin and A.R. Völkel, Phys. Rev. B **54** (1996) 12921.
- ⁶ G.M. Wysin, M.E. Gouvêa, A.R. Bishop and F.G. Mertens, in *Computer Simulations Studies in Condensed Matter Physics*, D.P. Landau et al., eds., (Springer-Verlag, Berlin, 1988).
- ⁷ M.E. Gouvêa, G.M. Wysin, A.R. Bishop and F.G. Mertens, Phys. Rev. B **39** (1989) 11840.
- ⁸ G.M. Wysin, Phys. Rev. B **49** (1994) 8780.
- ⁹ G.M. Wysin, submitted to Phys. Lett. A, May 14, 1997.
- ¹⁰ A.R. Pereira and A.S.T. Pires, Solid State Comm. **99**, 789 (1996); A.R. Pereira, F.O. Coelho and A.S.T. Pires, Phys. Rev. B **54**, 6084 (1996).
- ¹¹ Frustration makes consideration of out-of-plane vortex structure and calculation of critical anisotropy and the VIM impossible for the AFM triangular lattice.
- ¹² H.J. Mikeska, J. Phys. C**13**, 2913 (1980).
- ¹³ A.S.T. Pires and M.E. Gouvêa, Braz. J. Phys. **22**, 100 (1992).
- ¹⁴ Using our data from the ring Ansatz calculation, it is easy to get the in-plane vortex energy exactly, and fit to a logarithmic form. The cutoff $r_o \approx 0.22$ differs from that found in Ref.¹⁶ ($r_o \approx 2.12$).
- ¹⁵ See W.H. Press *et al.*, *Numerical Recipes*, Cambridge University Press (1986), or Steven E. Koonin and Dawn C. Meredith, *Computational Physics, Fortran Version*, Chapter 7, Addison-Wesley Publishing (1990), for a description of shooting schemes applied to Schrodinger problems.
- ¹⁶ C.E. Zaspel and D. Godinez, J. Magn. Magn. Mater. **162** (1996) 91.